



Soft Matter



Atomistic Simulation of Volumetric Properties of Epoxy Networks: Effect of Monomer Length

Journal:	<i>Soft Matter</i>
Manuscript ID	SM-ART-08-2021-001128.R1
Article Type:	Paper
Date Submitted by the Author:	24-Sep-2021
Complete List of Authors:	Khare, Ketan; Drexel University, Chemical and Biological Engineering Abrams, Cameron; Drexel University, Chemical and Biological Engineering

SCHOLARONE™
Manuscripts

Cite this: DOI: 00.0000/xxxxxxxxxx

Atomistic Simulation of Volumetric Properties of Epoxy Networks: Effect of Monomer Length[†]

Ketan S. Khare, ^a and Cameron F. Abrams ^{*a}

Received Date

Accepted Date

DOI: 00.0000/xxxxxxxxxx

Properties of epoxy thermosets can be varied broadly to suit design requirements by altering the chemistry of the component agents. Atomistically-detailed molecular dynamics simulations are well-suited for molecular insight into the structure-property relationship for a rational tailoring of the chemistry. Since the macroscopic properties of interest for applications emerge hierarchically from molecular-scale chemical interactions, seamless integration of experiment, computation, and theory is of great interest. Recently, a Specific Volume–Cooling Rate analysis protocol was successfully developed to quantitatively compare the volumetric properties of an epoxy network model with experimental results in the literature, in spite of the nine orders of magnitude mismatch in the accessible time-scales. Here, we extend the application of the method for two epoxy networks in the same class of chemistry but whose monomers have a higher number of repeating units compared to the previous one for validating the generality of our approach. We observed that atomistic simulations are able to predict the experimental temperature trend of the specific volume within 0.4% for both these networks. Using the William-Landel-Ferry equation to account for rate differences, we also see good agreement between the computational and experimental values of the glass transition temperature.

1 Introduction

The ability to alter the chemistry of the components enables a great versatility in the properties of thermosetting polymeric epoxy networks.¹ Such alterations can be made to either of the two components of the network: the epoxy monomer and the cross-linker. Relatively small changes in chemical details can have a drastic effect on the thermo-mechanical properties of the network.² Due to the ability to account for the effect of chemical interactions and topology explicitly, atomistically detailed molecular dynamics (MD) simulations together with experiments can be used to obtain and integrate a molecular-scale perspective with bulk thermo-mechanical properties.^{3–6} However, the inclusion of atomistic details is computationally expensive and limits the accessible time- and length-scales compared to typical thermo-mechanical analysis in experiments, and any mismatch in these scales need to be considered for comparison and integration.

Here, we are interested in the glass transition of such networks, which is commonly calculated from the temperature trend of specific volume during cooling from a high to a low temperature; i.e., from the rubbery to the glassy state. Due to the accessible time-scales, the typical computational cooling rates (\dot{q}_c 's) are $\sim 10^9 \text{ K s}^{-1}$ greater than experimental rates. As a result, the val-

ues of both the glassy specific volume (v_{sp}) and the glass transition temperature (T_g) obtained computationally are significantly higher than those obtained experimentally. Additionally, the computational glass transition is far broader than experiments, which complicates the identification of the rubbery and the glassy regions.^{7,8}

Recently, the Specific Volume–Cooling Rate analysis strategy was proposed to help overcome this obstacle.⁵ In that work, the chemistry of the epoxy network (Figure 1) was chosen based on the availability of extensive experimental data.^{9–12} In that work, we were able to objectively identify the rubbery state, since $v_{sp} - T$ trends would be \dot{q}_c -independent state points. Due to the vast mismatch in the rates, the lowest temperature with rubbery behavior in simulations was more than 150 K greater than the highest reported temperature for the $v_{sp} - T$ experimental trends. Nevertheless, a rubbery equation of state was obtained from the simulations and the experimental $v_{sp} - T$ trend was predicted within 0.3 %. Values of T_g as a function of \dot{q}_c were then calculated, and successfully compared with experimental behavior by involving the time–temperature superposition (TTS) principle.⁵ Unlike the comparison of T_g values, the extrapolation of the rubbery $v_{sp} - T$ trend is significantly more straightforward, which increases the confidence in the extent of agreement.

The need to test the generality of this approach has motivated us to pursue the study of epoxy networks composed of longer epoxy monomers with the same goal– the quantitative compar-

^a Department of Chemical and Biological Engineering, Drexel University, Philadelphia, Pennsylvania 19104, United States. * E-mail: cfa22@drexel.edu

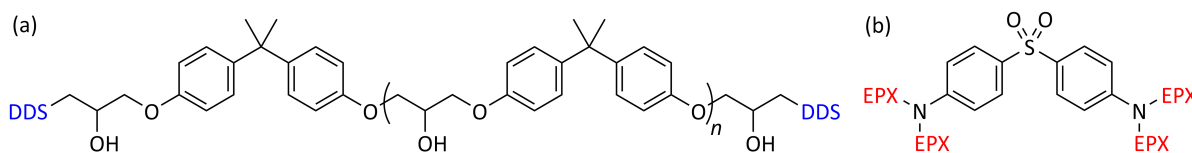


Fig. 1 Chemical Structure of (a) Monomer (EPX) units and (b) Cross-linker (DDS) units after network formation. As shown, each EPX unit is connected to two DDS units (blue), and each DDS unit is connected to four EPX units (red). For EPX, the number of repeating units (n) is 2, 5, and 11 for EP1, EP4, and EP7, respectively. EP1/DDS network was studied in the previous work.⁵

ison and integration of experiments^{9–12} and atomistic simulations. The length of the epoxy monomer (Figure 1) can be varied by altering the number of repeating units (n). As this value of n is increased, the cross-link density, the value of T_g and the density of the network show a decrease, as has been observed in experiments.^{9–12}

In this work, our goal is to quantitatively compare the computationally and experimentally obtained volumetric behavior directly by simulating atomistically detailed models of two additional networks, using the Specific Volume—Cooling Rate analysis strategy⁵ and experimental data from the literature.^{9–12} The remainder of this paper is organized as follows: In Section 2, we have discussed the details of the network chemistry, the model, the simulation details, and the analysis strategy. In Section 3, we have discussed our simulation results and compared them with experiments from the literature. And in the final section, we have summarized our findings.

2 Methods

The computational methods used here closely follow the previous work,⁵ but we have summarized them here for the sake of completeness. Furthermore, the methods used here are similar overall to those used to study various epoxy networks.^{5,6,8,13}

2.1 Chemistry

Two epoxy networks formed by the polycondensation of the oligomers of the diglycidyl ether of bisphenol-A (EPX) and 4,4'-diaminodiphenylsulfone (DDS) were studied here. In Figure 1, the chemical structure of the component units is shown after the formation of the EPX/DDS network. The number of repeating units n of EPX can be varied to modify the properties of the final cross-linked network. In previous work,^{5,6} we studied the model network formed by EPX with $n = 2$ and DDS using atomistic simulations. Based on those results, as discussed in the introduction, networks formed by EPX with $n = 5$ and $n = 11$ were of interest in this work. In the remainder of the text, EPX with $n = 2$, 5, and 11 is referred to EP1, EP4, and EP7, respectively. And correspondingly, the networks formed by these monomers and DDS are referred to as EP1/DDS, EP4/DDS, and EP7/DDS.

These values for n were specifically chosen due to the availability of relevant experimental data for equivalent systems in the literature^{9–12}. Specifically, EP1, EP4, and EP7 used in the EPX/DDS model networks are roughly equivalent respectively to Epon 1001F,¹⁴ Epon 1004F,¹⁵ and Epon 1007F,¹⁶ monomers in the EPON Resins¹⁷ product line. The experimental samples of the monomer are known to be polydisperse.^{9,10,14–16,18} However, since the polydispersity of the monomer has been shown to have

an insignificant effect on the properties of interest,¹⁸ the closest integer to the average value of n was used to model the EPX monomers for simplicity during structure preparation and analysis.

2.2 Simulation Details

All results reported in this work were obtained using all-atom atomistically detailed MD simulations. We used the general AMBER force field^{19–21} (GAFF) to describe the molecular interactions among atoms in the models. Partial charges in the atoms were calculated using the Austin Model 1—Bond Charge Correction^{22–24} (AM1-BCC) method. Both the GAFF and AM1-BCC method have been extensively used for cross-linked epoxy successfully.^{5,6,8,13,25–28} All simulations were performed using the Large-scale Atomic/Molecular Massively Parallel Simulator²⁹ (LAMMPS) simulation package. The van der Waals (vdW) interactions were calculated to a pairwise distance of 9 Å and then truncated. The residual effect on energy and pressure was calculated using tail corrections.³⁰ Coulombic interactions were calculated in the real-space up to a distance of 9 Å, beyond which the particle—particle particle—mesh³¹ (pppm) method was used. The Nosé-Hoover thermostat and barostat were used to maintain isothermal-isobaric conditions for the constant number of particles, pressure, temperature (NPT) simulations.^{32–34} All bonds and angles between atoms that included hydrogen atoms were constrained using the SHAKE³⁵ algorithm. A timestep of 1 fs was used for all the simulations. As was the case for the experiments,¹⁰ a pressure of 5 MPa was used. Additional details are available in our previous work.⁵

2.3 Structure Preparation

For creating the atomistic models of cross-linked epoxy, a liquid mixture of the monomer and cross-linker molecules was first simulated. An optimal connectivity sequence between the reacting atoms in this mixture was then identified. Using a multi-stage procedure, the monomers and the cross-linkers were then allowed to diffuse at an accelerated pace. Finally, after altering the local topology, MD simulation was used to relax the models of the polymer networks. These steps will be discussed in the subsequent paragraphs in greater detail.

Molecules of the monomer (EP4 or EP7) and the cross-linker (DDS) were added to a cubic simulation box in the stoichiometric ratio (Table 1). Based on our previous experience with reducing the effect of pressure fluctuations on the analysis of the volumetric properties in such systems,^{5,8} we have used a system size of about 200 000 atoms. Given that the EP4 and EP7 molecules are

Table 1 Details of the model networks for the different systems

System	No. of Monomers Molecules	No. of Cross-linkers Molecules	No. of Atoms
EP1/DDS ⁵	1458	729	212 139
EP4/DDS	784	392	210 504
EP7/DDS	420	210	216 090

longer than the EP1 molecules used in the previous work,⁵ the monomers were randomly oriented and sampled from the available conformational space in the initial box to ensure that the model was isometric. MD simulation was then performed to equilibrate the model of the mixture at a temperature of 800 K for a duration of 10 ns. Five independent replicas were obtained by using different seeds for the generation of the initial velocities of the atoms and also by using different initial conformations for the EP4 or EP7 molecules. All subsequent simulation and analysis steps were repeated for these five replicas of both systems.

As with the previous work,⁵ the connectivity sequence of the reacting atoms was identified from the mixture of the components in a single step, and then the network was gradually relaxed to obtain complete conversion. The relationship between the extent of conversion (or the degree of cure) and the viscoelasticity of cross-linked epoxy networks has been experimentally investigated in many works in the literature.^{36–41,41} We used the simulated annealing⁴² optimization algorithm to identify an optimal connectivity sequence between the terminal carbon atoms of the monomer and the nitrogen atoms of the cross-linkers with the objective of minimizing the sum of the square of the lengths between the connections.^{8,43,44} As with the previous work,⁵ while the vast majority of the proposed connections were less than 1 nm, a few proposed connections were as long as 2 nm. This distribution of the proposed connections reflects the highly cross-linked nature of the network, and in experiments the curing process at higher conversions is diffusion limited and required multiple hours to complete at temperatures above T_g . While accessible timescales in MD preclude an emulation of this process using natural diffusion, the ability (1) to perform simulations at exceptionally high temperatures and (2) to add biasing forces to the atoms in the network has been successfully exploited¹³ for creating the network as we have described below.

Using the optimized connectivity sequence, weak harmonic restraints were applied between the connecting atoms and the resulting model was simulated at a temperature of 800 K for a duration of 100 ps. From previous work, it is known that such a simulation is adequate for the molecular units to diffuse in response to the harmonic restraints without causing unphysical distortions of the topological and conformational integrity of the units. This process was then repeated in a series of 12 stages, where the harmonic restraints were progressively strengthened to the final values corresponding to the bond parameters for the monomer carbon atom and the cross-linker nitrogen atom according to the GAFF force field.^{19–21} This strategy of using progressively stronger harmonic restraints is called Directed Diffusion,¹³ and is conceptually analogous to advanced sampling techniques, which permit the MD simulation of thermodynamic processes that

would otherwise require timescales that are inaccessible. Indeed, a procedure conceptually similar to Directed Diffusion was recently devised for simulating a polymer network model for which the minimization of perturbations of the single-chain structural quantities when approaching complete conversion was especially important.⁴⁵ The specific schedule (i.e., the harmonic constant and the equilibrium length at each of the 12 stages) of the Directed Diffusion strategy that we used is identical to that used in the previous work.⁵

The stage-wise strengthening of these biasing forces has to be performed gently, because the restraints at each stage have the effect of tugging the connecting atoms and thus the components toward each other, and thus potentially stretching the individual molecular components. At each stage, the biasing forces are dissipated over the course of the simulation by the diffusion and conformational sampling of the components. Especially for flexible monomers, it is important to ensure that physically unrealistic stretching does not persist in the network and the network is able to relax. Hence, as a precaution, we used a somewhat higher temperature (800 K) and a longer simulation duration (100 ps) at each of the 12 stages than the previous work, where the those values for each stage were 700 K and 37.5 ps, respectively. While a discussion of the local dynamics of the networks is outside the scope of the present work and will be discussed in subsequent papers, the local dynamics of the networks⁶ at 800 K over a duration of 100 ps is ample for an efficient sampling of the system at each stage for the relaxation of the models.

After these 12 stages of simulation, all pairs of atoms subjected to harmonic forces in the connectivity sequence were separated roughly by the bond distance. The network was then “cross-linked” by altering the local topology (bonds, angles, dihedrals, and impropers) as specified by the force field.^{19–21} The partial charges of the atoms in the network were also adjusted to the final values calculated using the AM1-BCC method.^{22–24} The necessary alterations and adjustments were determined using a representative molecular model of the cross-link formed by the monomer and the cross-linker. This cross-linked model was then subjected to relaxation using MD simulation at a temperature of 820 K for a duration of 10 ns. No additional simulation was performed to achieve a target density. At the elevated temperature of 820 K, the model was observed to rapidly relax to a thermodynamic state point. These steps were performed for the five independent replicas for both systems.

The relaxation of the network models during this high temperature simulation was validated by the following additional checks: (1) the average value and fluctuations of the energy of the newly created internals (bonds, angles, dihedrals, and impropers) near the cross-linked sites were found to be consistent with the force field parameters; (2) the various thermodynamic quantities of the model reached a steady state over the course of the simulation; and (3) the five independent replicas for each system showed thermodynamic behavior that was statistically indistinguishable from that of the others.

2.4 Specific Volume—Cooling Rate Analysis

We then used the Specific Volume—Cooling Rate Analysis⁵ for the two systems. The key feature of this analysis is the use of different cooling rates to cool the model structures from the rubbery to the glassy state followed by a comparison of the resulting v_{sp} - T trends. Based on the previous work⁵ and experiments in the literature¹², the resulting v_{sp} - T trends are expected to show the following features while cooling: (1) cooling-rate independence at high temperatures (the rubbery region); (2) divergence from rubbery behavior (the transition region); and (3) cooling-rate independence of the slope of v_{sp} - T trends (the glassy region).

At high temperatures, the temperature trend of the specific volume is cooling rate-independent, since the trend corresponds to rubbery behavior. As the temperature decreases, the time required to reach equilibrium in response to a temperature change increases. At a temperature of T_1 , this time becomes insufficient and the v_{sp} diverges from the rubbery trend, i.e., the equation of state. Specifically, the v_{sp} will be higher than that expected from rubbery behavior. The values of T_1 decrease with a decrease in the cooling rate. As the temperature decreases, the v_{sp} - T trends undergo the glass transition and reach a temperature T_2 , below which the slope of the v_{sp} - T remains constant (thus, the coefficient of volumetric thermal expansion (α_v) is cooling-rate independent). Unlike T_1 values, the value of T_2 has been found to be cooling-rate independent for a given network.^{5,12}

Table 2 Cooling Rates used for Specific Volume—Cooling Rate Analysis. Experimental rate shown for comparison.

Designation	Cooling Rate (K s ⁻¹)	Simulation duration at each T step (ps)
1×	5.56×10^9	900
3×	1.67×10^{10}	300
9×	5.00×10^{10}	100
30×	1.67×10^{11}	30
Expt. ¹¹ (ref.)	5	N/A

Here, the two systems were cooled from a temperature of 820 K to 220 K at four different cooling rates in temperature steps of 5 K. The details about the four cooling rates are shown in Table 2. The final snapshots at temperatures of 400 K and 800 K from the 1× cooling rate simulations were then simulated for a duration of 50 ns to study the end-to-end distances (r_e) of the epoxy monomers and the cross-linkers. Although r_e calculations were performed after the Specific Volume—Cooling Rate analysis, we find it useful to begin the next section with a discussion on the relationship between r_e and n , since the only difference in the three networks is in the latter quantity.

3 Results and Discussion

3.1 End-to-End Distances of the Components in the Networks

Since the number of repeating units (n) was increased to vary the length of the epoxy monomer units, we were interested in the distribution of the end-to-end distance (r_e) of the epoxy monomers and the cross-linker units in the cross-linked network. After cross-linking/curing, the entire network is one single large molecule;

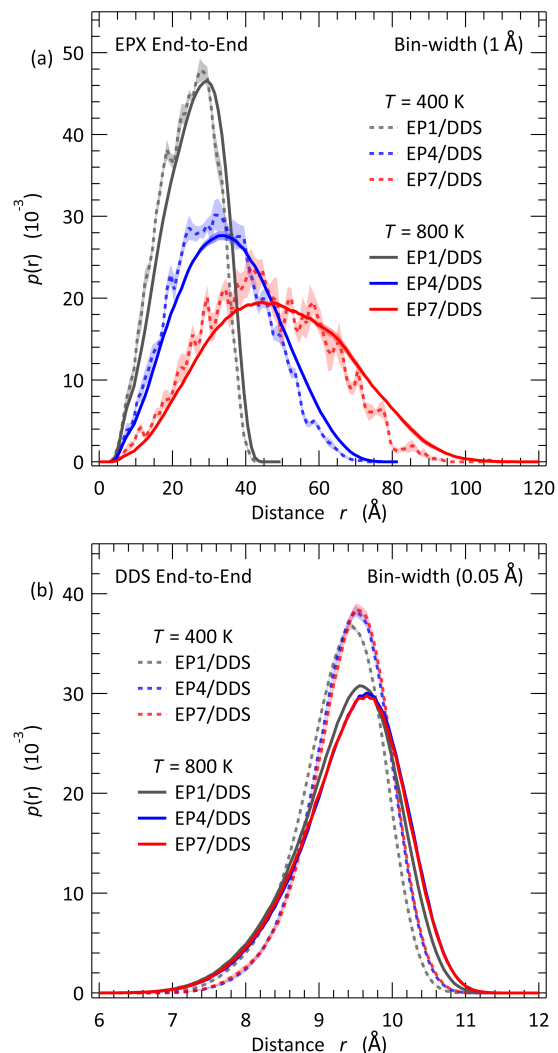


Fig. 2 Probability Density of the End-to-End distance (r_e) versus distance (r) of (a) epoxy monomers and (b) cross-linkers for the three networks at a temperature 400 K (glassy state) and 800 K (rubbery state). Uncertainty has been shown with shading.

however, it is convenient to analyze the differences in the epoxy monomer and cross-linker molecular units of the network because of their differing contributions to properties of the system. For the three systems, while the length of the monomer is varied, the cross-linker used is identical.

The r_e distributions were calculated for the three systems and are shown in Figure 2. As can be seen in part (a), the r_e distribution of the monomers for the three systems at 800 K is smooth and the five replicas are statistically indistinguishable from each other. There is a single peak. At a given temperature, as n increases, the peak value of the r_e of the monomer units increases and the distribution is broader. Compared to the distributions at the higher temperature (800 K), the distributions at the lower temperature show peaks at slightly shorter distances. More noticeable, however, is that the averaged distributions at the lower temperatures are not smooth compared to the higher temperature. This difference can be attributed to the absence of ergodicity at the lower temperature, which is a characteristic of the glassy state. Specif-

ically, the end-to-end distance of each monomer is invariant during the duration of the simulation below the glass transition.

From the chemical structures shown in Figure 1, it can be seen that unlike the relatively flexible epoxy monomers, the cross-linkers are short and rigid. The effect of this difference can be discerned by comparing parts (a) and (b) of Figure 2. While the r_e 's of the monomer units can vary by about 40 Å to 100 Å depending on the system, the r_e 's of the cross-linker units are narrowly distributed with a range of about 3 Å. For the cross-linkers, the distributions of r_e for the three systems at a given temperature is almost indistinguishable from each other. However, as expected, the distributions at a temperature of 400 K are slightly narrower than that at a higher temperature.

3.2 Specific Volume—Cooling Rate Trends

In Figure 3, the $v_{sp} - T$ trends at four different computational cooling rates for the EP4/DDS and EP7/DDS is shown in parts (a) and (b), respectively. The experimental $v_{sp} - T$ trends for the two networks obtained from the literature¹¹ are also shown in the corresponding parts of the same figure. The cooling rate used in the experiments (5 K s^{-1}) is more than nine orders of magnitude slower than the computational ones.⁽²⁾

The following observations are common for both networks. The simulation $v_{sp} - T$ trends remain cooling rate independent at the highest temperatures. Such independence is indicative of the state of thermodynamic equilibrium. At a cooling-rate dependent temperature designated T_1 , each $v_{sp} - T$ trend diverges from the slower ones. This divergence is seen to be modest initially, but becomes increasingly obvious as the temperature decreases. Consistently, the computational v_{sp} values obtained at a faster cooling rate deviate and are higher than slower ones. At a temperature of T_2 , the extent of divergence becomes constant. All of these observations for both networks are consistent with those of EP1/DDS studied computationally⁵ and experimentally.¹² For now, the specific values of T_1 's, T_2 's, and T_g 's are indicated in Figure 3 for facilitating this discussion. The criteria to calculate these values will be discussed subsequently.

Given the vastly faster computational cooling rates compared to experiments, the computational v_{sp} values are significantly higher than the experimental ones over the available range of the experimental data. The range of temperature of rubbery behavior for experiments is significantly below the corresponding range for the simulations. Thus, the rubbery $v_{sp} - T$ from experiments and simulations cannot be directly compared despite the expected rate-independence. However, by assuming a constant α_v above T_1 , a $v_{sp} - T$ equation of state can be calculated and extrapolated to lower temperatures. As can be seen for both networks, despite the need to extrapolate by 100 K due to the more than nine orders of magnitude difference in the cooling rates, we see excellent agreement between simulations and experiments. For both networks, the extrapolated v_{sp} values in the rubbery state are within 0.4 % of the experimental ones.

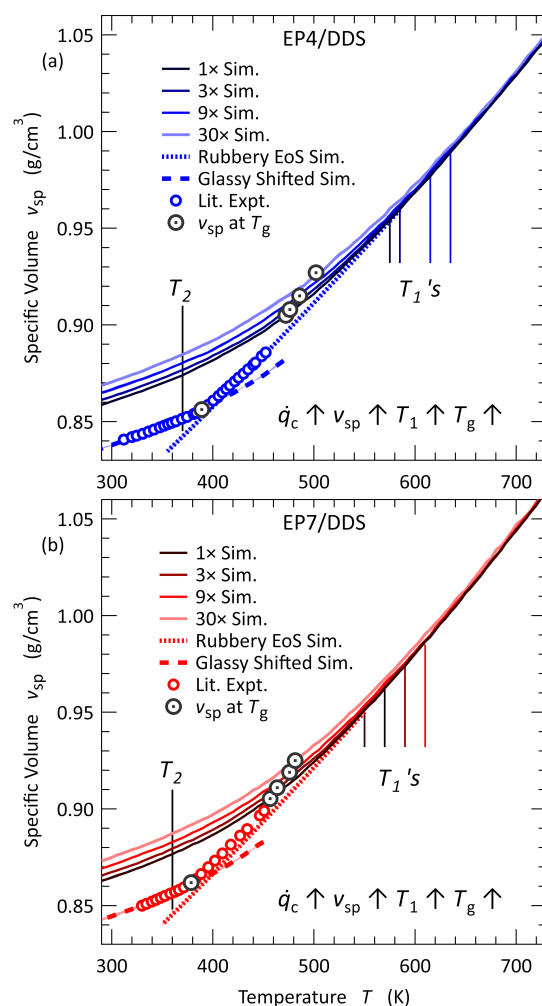


Fig. 3 Specific Volume (v_{sp}) versus temperature (T) of (a) EP4/DDS and (b) EP7/DDS. Trends were obtained for four different cooling rates using simulations, and the experimental trend was obtained from the literature.¹¹ Although the temperature range for the simulation was 820 K to 220 K, the range is truncated in the figure to focus on a specific range of interest. Uncertainty is less than the thickness of the lines.

3.3 Volumetric Thermal Expansion

From the $v_{sp} - T$ trends, the α_v can be calculated as $\alpha_v = \frac{1}{v_{sp}} \frac{\partial v_{sp}}{\partial T}$. For each of the four simulation trends, we used a tenth-order polynomial fit^{46,47} for each of the five replicas and obtain an average $\alpha_v - T$ trend. The resulting trend was compared with that obtained from a finite difference approximation of the derivative to check against numerical artifacts due to smoothing. The experimental $\alpha_v - T$ was obtained from the central difference approximation applied to the experimental dataset.¹¹ The trends for the two networks are shown in Figure 4.

The following observations are applicable for both networks. At the highest values of temperature (above T_1), the $\alpha_v - T$ trends are converged and are only very weakly dependent on temperature. The simulation trends are not sufficiently accurate to characterize the nature of the weak dependence, and we assume that the rubbery $\alpha_v - T$ trend is constant in the rubbery state. At $T \leq T_1$, the $\alpha_v - T$ trend begins to decay to a lower value. As expected, the transition begins at a lower temperature with a de-

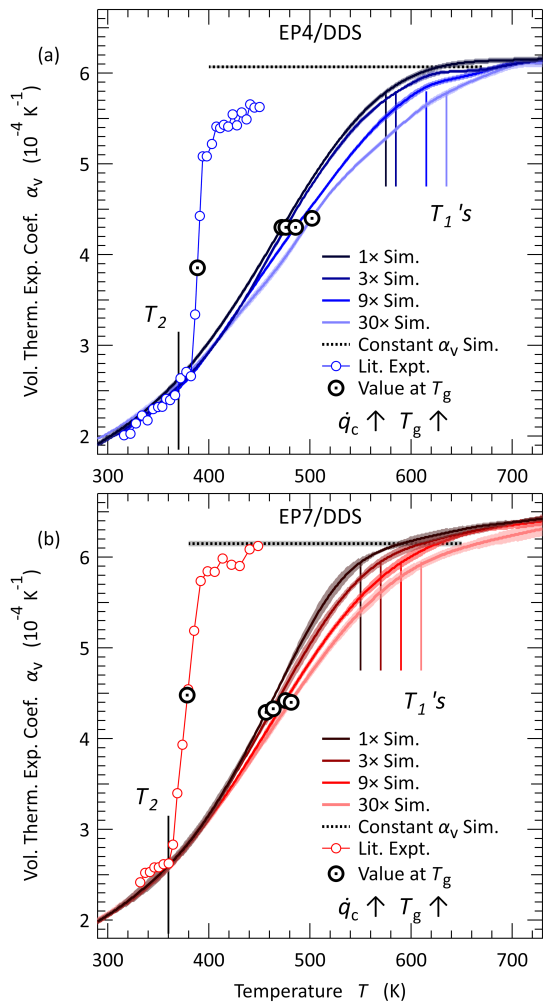


Fig. 4 Coefficient of volumetric thermal expansion (α_v) versus temperature (T) of (a) EP4/DDS and (b) EP7/DDS. This curves with open symbols are extracted from the work of Plazek.¹¹ Uncertainty has been shown with shading.

crease in the cooling rate. Compared to the simulation trends, the experimental trend shows a very sharp transition as would be expected given the vastly lower cooling rate. Below T_2 , the experimental and the four computational trends appear to converge. All these findings are consistent with the previous work on EP1/DDS.⁵

3.4 Determination of T_1 , T_2 , and T_g values

To calculate the values of T_g , it is necessary to find specific values of T_1 and T_2 for each of the $v_{sp} - T$ trends. In previous work,⁵ the onset of deviation in the $v_{sp} - T$ trends at a faster cooling rates from a slowest one was plotted and then the values of T_1 and T_2 were visually determined. Here, we have chosen to reduce the degree of subjectivity in the analysis by defining criteria based on $\alpha_v - T$ trends.

For both the model systems, we have calculated the average value of α_v between 650 K and 750 K using the trend obtained for 1× cooling rate. This temperature range is chosen because the $\alpha_v - T$ trends for both systems of the different cooling rates appear to converge in this range. For a given cooling rate, the

Table 3 T_1 , T_2 , and T_g values for EP4/DDS and EP7/DDS

Cooling Rate	T_1 (K)	T_2 (K)	T_g (K)
EP4/DDS			
1×	575	370	472.2 ± 0.88
3×	585	370	476.2 ± 1.44
9×	615	370	485.8 ± 1.53
30×	635	370	502.0 ± 2.1
Expt. ¹¹	408	370	389.04
EP7/DDS			
1×	550	360	456.7 ± 1.04
3×	570	360	463.7 ± 0.69
9×	590	360	475.9 ± 0.78
30×	610	360	481.4 ± 1.42
Expt. ¹¹	398	360	378.67

temperature at which the value of α_v reaches $0.95 \times \alpha_v$ is designated as T_1 . At this threshold, the decay of the $\alpha_v - T$ trends accelerate as can be seen in Figure 4. The value of T_2 is designated when all the $\alpha_v - T$ trends of the simulations and the experiment converge. Unlike T_1 , T_2 values are cooling rate independent, as discussed previously.^{5,12}

The value of T_g was calculated from the $v_{sp} - T$ trend of each of the five replicas as in the previous work.⁵ Linear fits to $v_{sp} - T$ trend were obtained in the rubbery (temperature range: $T_1 \leq T \leq T_1 + 100$) and in the glassy state (temperature range: $T_2 - 100 \leq T \leq T_2$). The value of T_g of each replica was designated to be the temperature at which the rubbery and glassy linear fits intersected. The average value for a system was calculated from the five replicas. All relevant values (T_1 's, T_2 's, and T_g 's) for both the systems are shown in Table 3, and also marked in Figures 3 and 4.

As the cooling rate increases, the networks have a shorter time to sample the conformational space. Accordingly, the values of T_1 increase with an increase in the cooling rate for both systems. On the other hand, the value of T_2 for each system appears to be cooling rate independent. This observation has been previously reported in experiments¹² and simulations.⁵ Accordingly, the values of T_g for each system consistently increase with an increase in the cooling rate. Finally, in Figure 5, we show the departure of the specific volume (δv_{sp}) as a function of temperature for the two systems. The δv_{sp} value at a given temperature above or below the T_g is the difference between the v_{sp} and the linear fit to the rubbery or the glassy $v_{sp} - T$ trend. As can be seen in Figure 5, the breadth of the glass transition increases with an increase in the cooling rate. Interestingly, the peak value of the δv_{sp} , which occurs at T_g , appears to be similar for a given cooling rate for all three systems.⁵ Additionally, for each system the trends appear to be self-similar. Similar observations can be made for the EP1/DDS published previously.⁵ We acknowledge that different criteria can be employed to designate the values of T_1 and T_2 , but the resulting differences in the value of T_g will be modest. Our focus here is not to define universal criteria for T_1 or T_2 , but to propose useful criteria that can be applied consistently for the systems studied here. With further progress in computational work, it may be possible to refine such criteria.

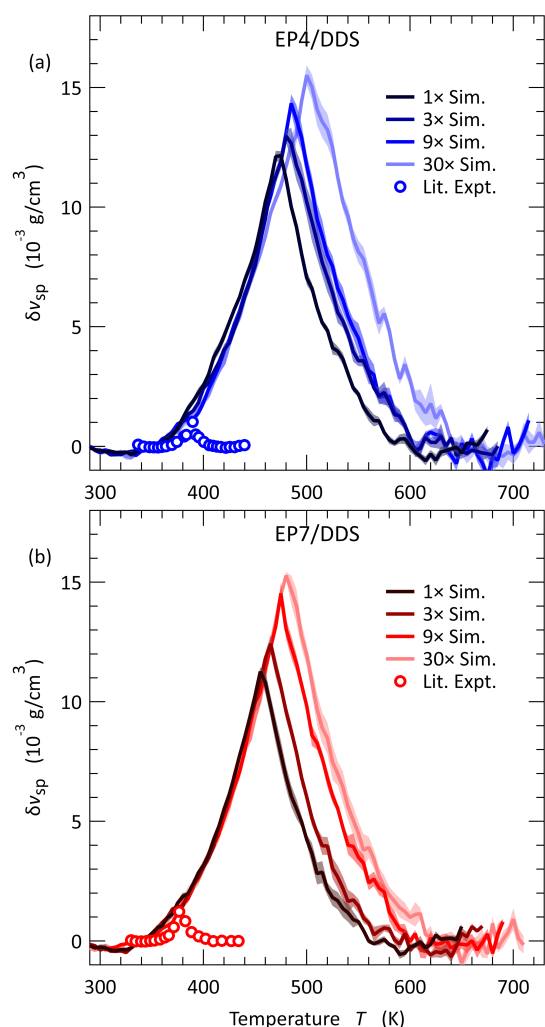


Fig. 5 Departure of specific volume (δv_{sp}) versus temperature (T) of (a) EP4/DDS and (b) EP7/DDS for the four simulation cooling rates. These curves with open symbols are extracted from the work of Plazek.¹¹ Uncertainty has been shown with shading.

3.5 Comparison of the Three Networks

In Figure 6(a), the computational and experimental $v_{sp} - T$ trends of the three networks are compared. For visual simplicity, we only used the slowest computational cooling rate ($1\times$) trend. In the same figure, we show the rubbery prediction as well. As expected, the values of v_{sp} of the network composed of the longer monomer are consistently higher at a given temperature for both experiments and simulations. The computational and experimental trends diverge from the rubbery line at a lower temperature as the monomer length increases. And correspondingly, the values of T_g are lower as the monomer length increases.

In Figure 6(b), the $\alpha_v - T$ trends of the three networks are shown corresponding to the $v_{sp} - T$ trends in part (a). For the simulation trends, it can be seen clearly that the value of α_v at a given temperature is higher as the monomer length increases. This is also evident for the experimental trends and discussed in the literature.¹¹

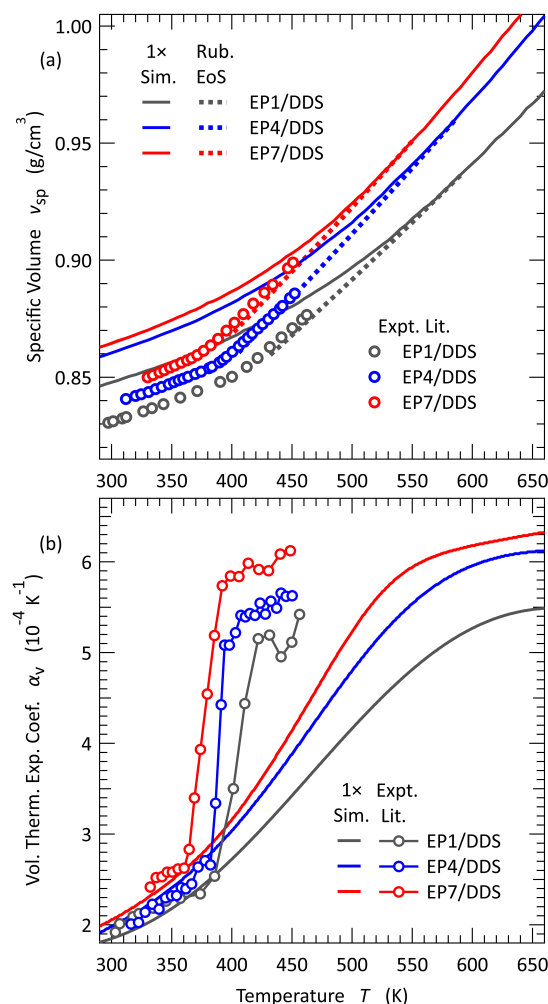


Fig. 6 EP1/DDS,⁵ EP4/DDS, and EP7/DDS networks ($n = 2, 5$, and 11 , respectively). (a) v_{sp} versus T (b) α_v versus T . For simulations, only the slowest cooling rate ($1\times$) trend is shown.

3.6 Time—Temperature Superposition

The quantitative application of the TTS principle is accomplished by the calculation of the time-shift factor (a_T) at some temperature (T) with respect to some convenient reference temperature (T_{ref}). The $a_T - T$ trend is often used to parameterize the William-Landel-Ferry (WLF) equation:^{48,49}

$$\log_{10} a_T = \log_{10} \frac{\dot{q}_{ref}}{\dot{q}_T} = \frac{-C_1(T - T_{ref})}{C_2 + (T - T_{ref})}, \quad (1)$$

where \dot{q}_{ref} and \dot{q}_T are the cooling rates such that $T_g = T_{ref}$ and $T_g = T$ respectively; C_1 and C_2 are system-specific WLF parameters. The experimental time-shift factors and the WLF parameters (Table 4) were obtained from the literature.^{10–12}

Table 4 WLF Parameters for the Three Networks^{10–12}

System	C_1	C_2	T_{ref} (K)
EP1/DDS	19.26	50	403.2
EP4/DDS	21.02	50	384.0
EP7/DDS	20.50	50	373.9

While the WLF equation is an empirical relationship, the equa-

tion has been successfully used to extrapolate and bridge the large gap between the shortest time-scales investigated by experiments and the longest time-scales that can be accessed via simulations for polymers, in general,⁵⁰ and for epoxy networks, in particular.^{5,6} In Figure 7, the values of a_T of experiments and the WLF relationship for the three networks, are compared with the values of T_g calculated from simulations in this work. As can be seen in the figure, the a_T values of EP4/DDS and EP7/DDS from simulations show good agreement with the WLF extrapolation. As can be seen in the figure, there is a gap in the temperature range of more than 100 K, which corresponds to the vast mismatch in the accessible timescales of experiments and simulations. This gap is bridged using the WLF equation. Thus, given the context of the quantitative comparison, the agreement between the simulations and the experiments is highly satisfactory.

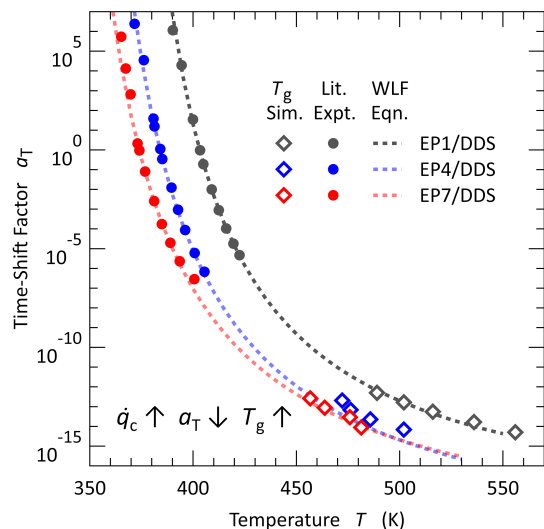


Fig. 7 Time-shift factors (a_T) versus temperature (T) for the three networks are shown. Experimental values (circles) and WLF parameters (dashed lines) were obtained from the literature.^{11,12} EP1/DDS was studied previously.⁵ Three colors are used to correspond to each of the three networks.

3.7 Comparison of Experiments and Simulations

In Table 5, the density ($\rho = v_{sp}^{-1}$) for the three systems from experiments^{10–12} and simulations are compared for both the rubbery ($T = 450$ K) and the ($T = 330$ K) glassy states. Conceptually, the equilibrium density obtained via experiments and simulations in the rubbery state should be identical, since rate effects are irrelevant. As discussed in section 3.2, the rubbery $v_{sp} - T$ trend from simulations was extrapolated to lower temperatures. As can be seen in the table for the rubbery state, the difference in the ρ values between the experiments and simulations for the EP1/DDS, EP4/DDS, and EP7/DDS is -0.3% , -0.1% , and -0.4% , respectively. This difference compares very favorably with a study⁵¹ reporting the application of GAFF^{19–21} for molecular property prediction of 65 organic compounds, where the average unsigned error in the ρ values from simulations compared to the experiments was found to be 3.43%. Similarly, a more recent work⁵² on ionic liquids using GAFF^{19–21} for simulations was found to predict the

density within 1% to 4% of the experimental values. Thus, we conclude that excellent agreement is seen between the prediction from simulations and the experiments for all three systems.^{10–12} Furthermore, since this prediction involved the use of extrapolation, it can be concluded that our simulations also successfully captured the temperature dependence of the density.

In the glassy state, the rates used to cool the network from the rubbery to the glassy state will affect the density. The density from the experiments is expected to be higher due to the vastly higher cooling rates used in simulations. As can be seen in the table, the difference in the glassy state density between the experiments and simulations ($1 \times$ cooling rate) for the EP1/DDS, EP4/DDS, and EP7/DDS is 2.0%, 2.6%, and 2.3%, respectively. These values are comparable to the difference (1.9% to 3.3%) seen for other cross-linked epoxy networks.^{8,13,44} Furthermore, as can be inferred from Figure 3, this difference in the glassy state density of the experiments and the simulations increases consistently for the three systems as the difference in the cooling rate increases to about 5%. Unlike the case in the rubbery state, this difference in density between experiments and simulations is the result of the rate effect on the properties of polymer networks, and must not be classified as an error. As the cooling rate increases, the glassy state density is expected to be lower. The ability to successfully capture this dependence is crucial for obtaining the cooling rate dependence of the T_g that was discussed in section 3.6.

Table 5 Comparison of Experiments^{10–12} and Simulations ($1 \times$ cooling rate) for the three systems. Temperature $T = 450$ K for the rubbery state, $T = 330$ K for the glassy state. Simulation v_{sp} values were extrapolated as discussed in section 3.2. Uncertainty from simulations is less than 0.001 g cm^{-3}

System	ρ_{rubbery} (g cm^{-3})		ρ_{glassy} (g cm^{-3})	
	Exp.	Sim. EoS	Exp.	Sim.
EP1/DDS ⁵	1.148	1.1511	1.197	1.1725
EP4/DDS	1.130	1.1310	1.186	1.1550
EP7/DDS	1.114	1.1191	1.176	1.1494

Potentially, there are several sources of errors or discrepancies that could adversely affect the agreement between experiments and simulations. Other than the approximations underlying GAFF^{19–21}, the AM1-BCC method^{22–24}, and other simulation details, some factors are peculiar to polymer networks. Experimental materials may have measurable impurities or may be poly-disperse.¹⁰ The network formation in experiments could also be affected by diffusion limitation, side reactions, or thermal degradation.¹⁰ The network topology created in the experiments may deviate from the computational model. However, these factors do not appear to hamper the comparison of experiments and simulations in our work. Overall, we conclude that the volumetric properties studied via simulations show excellent agreement with the experiments for the three systems.

4 Conclusions

Atomistic MD simulation of cross-linked epoxy has continued to be a vigorous area of research.^{3,53–61} Additionally, there has been

considerable interest in performing coarse-grained as well as hierarchical simulations of cross-linked epoxy to model longer length- and time-scales.^{3,62,63} In this work, we have prepared atomistic models of two epoxy networks composed of EP4/DDS and EP7/DDS. For improving the certainty of the calculations, we have used five independent replicas and a large system size for the models of the networks.^{4,5,8} We have studied the volumetric properties using MD simulations and compared our results with experiments in the literature.^{10–12} This work extends our previous work⁵ on EP1/DDS in which a Specific Volume—Cooling Rate analysis was proposed to successfully compare atomistic simulations and experiments despite the vast mismatch in the accessible time-scales.

Here, we have validated our previously developed analysis strategy for two more networks. We have successfully compared the computational and experimental $v_{sp} - T$ trends as well as the values of T_g . The advantage of successfully comparing the $v_{sp} - T$ trends is that such comparison significantly reduces any impact of interpretation of the simulation data. Nevertheless, the successful comparison of T_g 's captures the relationships among the conformational entropy, the network topology, cohesive intermolecular forces, and available time-scale for relaxation. We are currently working on studying the local translation dynamics for these networks using simulations and integrating our calculations with experimentally obtain creep compliance, in a similar manner as was done for EP1/DDS.⁶

Author Contributions

Ketan S. Khare: Conceptualization; Methodology; Software; Investigation; Formal Analysis; Resources; Visualization; Writing – original draft; Writing – review and editing. **Cameron F. Abrams:** Conceptualization; Formal Analysis; Resources; Supervision; Writing – review and editing; Funding acquisition.

Conflicts of interest

There are no conflicts to declare.

Acknowledgements

Research was sponsored by the United States Army Research Laboratory and was accomplished under Cooperative Agreement Number W911NF-14-2-0227. The views and conclusions contained in this document are those of the authors and should not be interpreted as representing the official policies, either expressed or implied, of the United States Army Research Laboratory or the U.S. Government. The U.S. Government is authorized to reproduce and distribute reprints for Government purposes notwithstanding any copyright notation herein. Certain commercial materials are identified in this article to foster understanding. Such identification does not imply recommendation or endorsement by the authors.

Simulations were performed in part using computational resources provided by the Open Research Service (ORS), High Performance Computing Modernization Program (HPCMP) of the United States Department of Defense. This work also used the Extreme Science and Engineering Discovery Environment (XSEDE) Stampede2 at the Texas Advanced Supercomputing Cen-

ter through allocation TG-MCB070073N. XSEDE is supported by National Science Foundation grant number ACI-1548562.

References and Notes

- 1 H. Q. Pham and M. J. Marks, in *Ullmann's Encyclopedia of Industrial Chemistry*, Wiley-VCH, Weinheim, 3rd edn, 2005, vol. 13, pp. 155–244.
- 2 A. C. Grillet, J. Galy, J.-F. Gérard and J.-P. Pascault, *Polymer*, 1991, **32**, 1885–1891.
- 3 C. Li and A. Strachan, *J. Polym. Sci., Part B: Polym. Phys.*, 2015, **53**, 103–122.
- 4 T. E. Gartner and A. Jayaraman, *Macromolecules*, 2019, **52**, 755–786.
- 5 K. S. Khare and F. R. Phelan Jr., *Macromolecules*, 2018, **51**, 564–575.
- 6 K. S. Khare and F. R. Phelan Jr., *Macromol. Theory Simul.*, 2020, **29**, 1900032.
- 7 P. N. Patrone, A. Dienstfrey, A. R. Browning, S. Tucker and S. Christensen, *Polymer*, 2016, **87**, 246–259.
- 8 T. W. Sirk, K. S. Khare, M. Karim, J. L. Lenhart, J. W. Andzelm, G. B. McKenna and R. Khare, *Polymer*, 2013, **54**, 7048–7057.
- 9 J. D. Lemay, B. J. Swetlin and F. N. Kelley, in *Characterization of Highly Cross-linked Polymers*, ACS Symposium Series, American Chemical Society, Washington, DC, 1984, vol. 243, ch. 10, pp. 165–183.
- 10 I.-C. Choy and D. J. Plazek, *J. Polym. Sci., Part B: Polym. Phys.*, 1986, **24**, 1303–1320.
- 11 D. J. Plazek and I. C. Choy, *J. Polym. Sci., Part B: Polym. Phys.*, 1989, **27**, 307–324.
- 12 C. A. Bero and D. J. Plazek, *J. Polym. Sci., Part B: Polym. Phys.*, 1991, **29**, 39–47.
- 13 K. S. Khare and R. Khare, *Macromol. Theory Simul.*, 2012, **21**, 322–327.
- 14 Hexion Inc., *EPON™ Resin 1001F Technical Data Sheet*, 2020.
- 15 Hexion Inc., *EPON™ Resin 1004F Technical Data Sheet*, 2020.
- 16 Hexion Inc., *EPON™ Resin 1007F Technical Data Sheet*, 2020.
- 17 Registered Trademark of Hexion Inc. Corporation, 180 East Broad St., Columbus OH 43215, United States.
- 18 I. M. McAninch, *Molecular Toughening of Epoxy Networks*, PhD Thesis, Drexel University, Philadelphia, PA, USA, 2014.
- 19 J. Wang, W. Wang, P. A. Kollman and D. A. Case, *J. Mol. Graphics Modell.*, 2006, **25**, 247–260.
- 20 J. Wang, R. M. Wolf, J. W. Caldwell, P. A. Kollman and D. A. Case, *J. Comput. Chem.*, 2004, **25**, 1157–1174.
- 21 General AMBER Force Field (Version 1.8, March 2015) included in AmberTools 16.
- 22 M. J. S. Dewar, E. G. Zebisch, E. F. Healy and J. J. P. Stewart, *J. Am. Chem. Soc.*, 1985, **107**, 3902–3909.
- 23 A. Jakalian, B. L. Bush, D. B. Jack and C. I. Bayly, *J. Comput. Chem.*, 2000, **21**, 132–146.
- 24 A. Jakalian, D. B. Jack and C. I. Bayly, *J. Comput. Chem.*, 2002, **23**, 1623–1641.
- 25 C. Jang, T. W. Sirk, J. W. Andzelm and C. F. Abrams, *Macromol. Theory Simul.*, 2015, **24**, 260–270.

- 26 M. Sharifi, C. Jang, C. F. Abrams and G. R. Palmese, *Macromolecules*, 2015, **48**, 7495–7502.
- 27 A. S. Sridhar and C. F. Abrams, *J. Dynamic Behavior Mater.*, 2019, **5**, 143–149.
- 28 A. Srikanth and C. F. Abrams, *Comput. Mater. Sci.*, 2019, **169**, 109082.
- 29 S. Plimpton, *J. Comput. Phys.*, 1995, **117**, 1–19.
- 30 H. Sun, *J. Phys. Chem. B*, 1998, **102**, 7338–7364.
- 31 R. W. Hockney and J. W. Eastwood, *Computer Simulation Using Particles*, Institute of Physics Publishing, Philadelphia, 1988, pp. 267–301.
- 32 S. Nosé, *J. Chem. Phys.*, 1984, **81**, 511–519.
- 33 W. G. Hoover, *Phys. Rev. A*, 1985, **31**, 1695–1697.
- 34 W. Shinoda, M. Shiga and M. Mikami, *Phys. Rev. B*, 2004, **69**, 134103.
- 35 J.-P. Ryckaert, G. Ciccotti and H. J. C. Berendsen, *J. Comput. Phys.*, 1977, **23**, 327–341.
- 36 G. Wisanrakkit and J. K. Gillham, *J. Appl. Polym. Sci.*, 1990, **41**, 2885–2929.
- 37 J. O. Simpson and S. A. Bidstrup, *J. Polym. Sci., Part B: Polym. Phys.*, 1995, **33**, 55–62.
- 38 B. G. Min, Z. H. Stachurski and J. H. Hodgkin, *Polymer*, 1993, **34**, 4488–4495.
- 39 J. B. Enns and J. K. Gillham, *J. Appl. Polym. Sci.*, 1983, **28**, 2567–2591.
- 40 B. G. Min, Z. H. Stachurski, J. H. Hodgkin and G. R. Heath, *Polymer*, 1993, **34**, 3620–3627.
- 41 M. J. Marks and R. V. Snelgrove, *ACS Appl. Mater. Interfaces*, 2009, **1**, 921–926.
- 42 S. Kirkpatrick, C. D. Gelatt and M. P. Vecchi, *Science*, 1983, **220**, 671–680.
- 43 R. Khare, M. E. Paulaitis and S. R. Lustig, *Macromolecules*, 1993, **26**, 7203–7209.
- 44 P.-H. Lin and R. Khare, *Macromolecules*, 2009, **42**, 4319–4327.
- 45 G. M. Tow and E. J. Maginn, *Macromolecules*, 2021, **54**, 4488–4496.
- 46 MATLAB, version 9.9.0 (R2020b), MathWorks Inc., Natick, MA, United States, 2020.
- 47 MathWorks Inc., *Curve Fitting Toolbox*, Natick, MA, United States, 2020.
- 48 M. L. Williams, R. F. Landel and J. D. Ferry, *J. Am. Chem. Soc.*, 1955, **77**, 3701–3707.
- 49 J. Ferry, in *Viscoelastic Properties of Polymers*, Wiley, New York, 3rd edn, 1980, ch. 11, pp. 264–320.
- 50 A. Soldera and N. Metatla, *Phys. Rev. E*, 2006, **74**, 061803.
- 51 J. Wang and T. Hou, *J. Chem. Theory Comput.*, 2011, **7**, 2151–2165.
- 52 K. G. Sprenger, V. W. Jaeger and J. Pfendtner, *J. Phys. Chem. B*, 2015, **119**, 5882–5895.
- 53 B. Demir and T. R. Walsh, *Soft Matter*, 2016, **12**, 2453–2464.
- 54 S. V. Kallivokas, A. P. Sgouros and D. N. Theodorou, *Soft Matter*, 2019, **15**, 721–733.
- 55 C. Li and A. Strachan, *Polymer*, 2018, **135**, 162–170.
- 56 F. Vuković and T. R. Walsh, *ACS Appl. Mater. Interfaces*, 2020, **12**, 55278–55289.
- 57 S. C. Chowdhury, R. Prosser, T. W. Sirk, R. M. Elder and J. W. Gillespie, *Appl. Surf. Sci.*, 2021, **542**, 148738.
- 58 S. S. Bamane, P. S. Gaikwad, M. S. Radue, S. Gowtham and G. M. Odegard, *Polymers (Basel, Switz.)*, 2021, **13**, 2162.
- 59 A. Shundo, M. Aoki, S. Yamamoto and K. Tanaka, *Macromolecules*, 2021, **54**, 5950–5956.
- 60 A. M. Hubbard, Y. Ren, D. Konkolewicz, A. Sarvestani, C. R. Picu, G. S. Kedziora, A. Roy, V. Varshney and D. Nepal, *ACS Appl. Polym. Mater.*, 2021, **3**, 1756–1766.
- 61 C. W. Jang, J. H. Kang, F. L. Palmieri, T. B. Hudson, C. J. Brandenburg and J. W. Lawson, *ACS Appl. Polym. Mater.*, 2021, **3**, 2950–2959.
- 62 Y. Kawagoe, G. Kikugawa, K. Shirasu and T. Okabe, *Soft Matter*, 2021, **17**, 6707–6717.
- 63 J. J. Schichtel and A. Chattopadhyay, *Comput. Mater. Sci.*, 2020, **174**, 109469.